Electronic Supplementary Information (ESI)

Nitrogen-doped heterostructure carbon functionalized by electroactive organic molecules for asymmetric supercapacitors with high energy density

Bingshu Guo, Zhongai Hu, Yufeng An, Ning An, Pengfei Jia, Yadi Zhang, Yuying Yang, Zhimin Li.*

Key Laboratory of Eco-Environment-Relatged Polymer Materials of Ministry of Education, Key Laboratory of Polymer Materials of Gansu Province, College of Chemistry and Chemical Engineering, Northwest Normal University, Lanzhou 730070, PR China

1. Introduction

In order to prove the unzipped carbon nanotubes have good dispersion, we have prepared the aqueous dispersions of the Multi-walled carbon nanotubes (MWCNTs) and heterostructure carbon nanotubes (HCNTs) with same concentration (0.1 mg mL^{-1}). After sonication for 30 min, the HCNTs were homogeneously dispersed to form a black solution, while the pristine MWCNTs suspended themselves in the water (Fig. S1a). After a week, the dispersed solution still keeps homogeneous for the HCNTs while the sedimentation is obviously seen for the MWCNTs (Fig. S1b). For comparing the hydrophilicity, the contact angle measurements of MWCNTs and HCNTs were also provided. Seen from Fig S1c and Fig S1d, the corresponding contact angle for the MWCNTs is about 131.7° indicating that the MWCNTs are hydrophobic material. But for HCNTs, the contact angle is nearly 0°. This suggests

*Corresponding author. Tel.: +86 931 7973255; Fax: +86 931 8859764.
E-mail address: zhongai@nwnu.edu.cn (Zhong-ai Hu)

that the HCNTs are completely hydrophilic, which is propitious to the accessibility of electrolyte ions to active sites during the electrochemical process. Moreover, in order to certify the specific surface area of HCNTs were increased, we have performed the BET measurement (Fig. S1e). It inferred from the BET analysis that the specific surface area of HCNTs (185.3 m^2 g^{-1}) is really larger than that of MWCNTs (102.3 m^2 g^{-1}), which is consistent with the relevant literatures as shown in Table S1

2. Structure characterization

2.1. FT-IR

Fig S2 shows the FT-IR spectrum of NHC. The broad and intense absorption band at around 3430 and 1608 cm^{-1} could be interpreted as O-H stretching vibrations and deformation vibrations of the water molecules.[15] However, the N-H stretching vibration band at about 3300 cm^{-1} becomes inconspicuously, which may be covered by the absorption bond of O-H stretching vibrations. The bands at about 2925, 1398 and 1262 cm^{-1} are assigned to C-H stretching vibration, C-O-C (epoxy) stretching vibration and C-N stretching vibration of a secondary amine from NHC, respectively.[16] Besides, the bond near 802 cm^{-1} corresponds to aromatic C-H out-of-plane deformation vibration.

3. Electrochemical Characterization

3.1 Contents calculation

A segment of the cyclic voltammogram at a scan rate of 20 mV s^{-1} was integrated according to the equation (1) and (2):

$$Q = \int Idt = \int_{V_a}^{V_b} \frac{I}{\frac{dV}{dt}} dV = \frac{1}{v}\int_{V_a}^{V_b} IdV \qquad (1)$$

$$m_A = n_A M_A = \frac{Q}{zF} M_A \qquad (2)$$

where Q (C), V (V), I (A), t (s), m_A (g), n_A (mol), M_A (mol g^{-1}), F and z represent voltammetric charge, potential, instantaneous anodic (cathodic) current, sampling time, mass of the material that takes part in redox reactions, amount of substance, molar mass, Faraday constant and stoichiometric coefficient of electron transport in the electrochemical processes, respectively. The V_a (V) and V_b (V) are defined as the selected boundaries of potential range. The Q is numerically equal to the integral area of the dash area as shown in Fig S5 (a and b). The calculations indicated that the contents of TCBQ and AQ are about 22.1% and 18.6% of the total mass in the optimal sample, respectively.

Fig. S6a displays the CV curves of TCBQ-NHC with different mass ratio at a scan rate of 10 mV s^{-1}. When the content of TCBQ-NHC is relatively low (1:4 and 1:5), the CV curves show a single redox couple at the potential about 0.5 V. With increasing of the content of TCBQ (1:3), the CV curve appears the other pair of shoulder peaks at the potential around 0.4 V. At this point, the electrode has a maximum specific capacitance of 365 F g^{-1} with the current density at 1 A g^{-1}. As the TCBQ content continues increase (1:2), the peak intensity of TCBQ-NHC is gradually weakened. The specific capacitances of TCBQ-NHC with different mass ratio are shown in Fig S6b. For AQ-NHC, with increasing of the content of AQ-NHC (1:4 to 1:2), the shapes of the CV curve have almost no obverse change (Fig S6c).

Meanwhile, the specific capacitances of AQ-NHC with different mass ratio are presented in Fig S6d. Among them, the maximum specific capacitance of 331 F g^{-1} is achieved when the AQ-NHC content is 1:4.

In addition, we also directly used HCNTs as substrate to absorb AQ through refluxing to achieve AQ functionalized HCNTs (AQ-HCNTs). Fig S7 shows a series results of electrochemical measurements. As shown in Fig S7a, the CV curves display a couple of redox peaks with oxidation and reduction peaks locating at the potential near -0.09 and -0.11 V, respectively. Fig. S7b gives the galvanostatic charge-discharge (GCD) curves of the HCNTs and AQ-HCNTs at the current density of 1A g^{-1}. Based on calculation, the HCNTs show the specific capacitance of 165 F g^{-1}, which is approximately 10 times larger than the pristine MWCNTs (12 F g^{-1}). After modifying, the specific capacitance of AQ-HCNTs is 285 F g^{-1}. When the current density is 20 A g^{-1}, the specific capacitance retentions of MWCNTs, HCNTs and AQ-HCNTs are 51.4%, 71.5% and 71.2% of the initial value at 1 A g^{-1}.

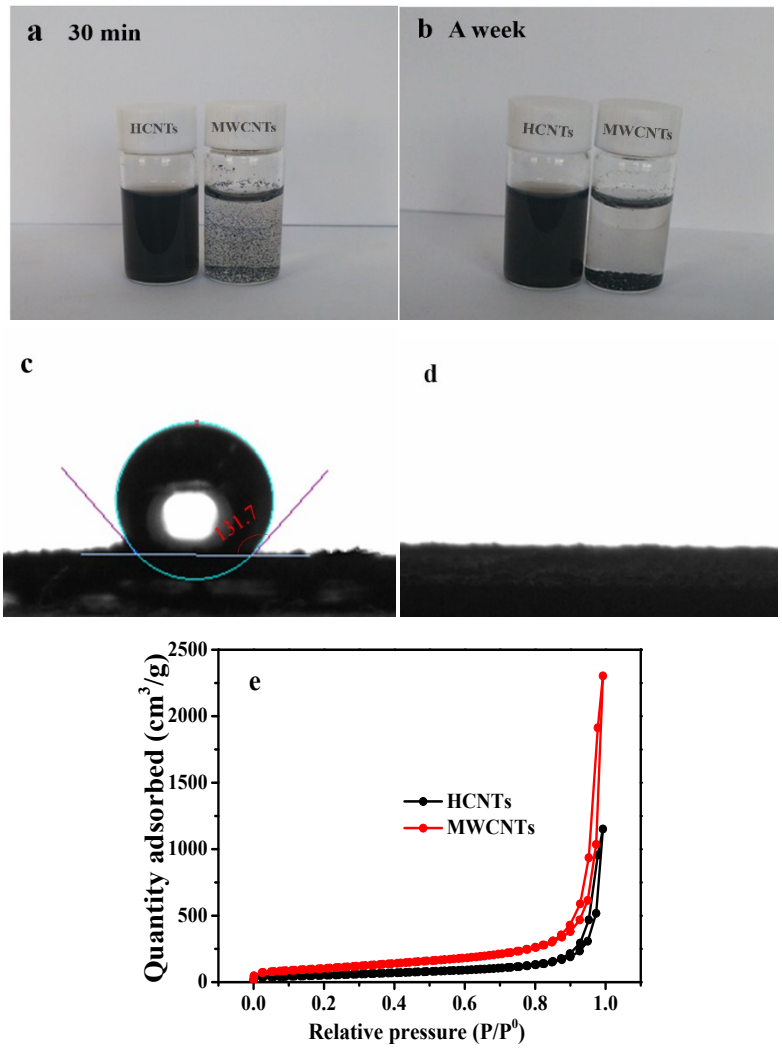

Fig. S1 Photographs of aqueous dispersions of MWCNTs and HCNTs (a, b) at a concentration of 0.1 mg mL^{-1}, contact angle measurements of MWCNTs (c), and HCNTs (d), Nitrogen adsorption/desorption isotherms of MWCNTs and HCNTs (e).

Table S1. Specific surface area and specific capacitance comparison of different materials.

Pristine MWCNTs ($m^2 g^{-1}$)	Dissected MWCNTs ($m^2 g^{-1}$)	Specific capacitance ($F g^{-1}$)	Ref (year)	Porous carbon ($m^2 g^{-1}$)	Specific capacitance ($F g^{-1}$)	Ref (year)
47	85	256@0.3 A g^{-1}	1 (2012)	1084	308@1 A g^{-1}	8 (2015)
17.6 ± 2.4	33.1 ± 0.3	232.9@1A g^{-1}	2 (2013)	1580	855 @1 A g^{-1}	9 (2015)
172	391	152 @ 1 A g^{-1}	3 (2011)	2572	228 @1 A g^{-1}	10 (2015)
291	511	_	4 (2010)	1938	254 @1 A g^{-1}	11 (2015)
47.3	321.6	_	5 (2014)	1749	313 @1 A g^{-1}	12 (2015)
93	120	_	6 (2014)	2080	304 @ 1 A g^{-1}	13 (2014)
30	161	_	7 (2014)	2988	306 @1 A g^{-1}	14 (2015)
102.1	185.3	165 @ 1A g^{-1}	This work	1454	251 @ 1A g^{-1}	This work

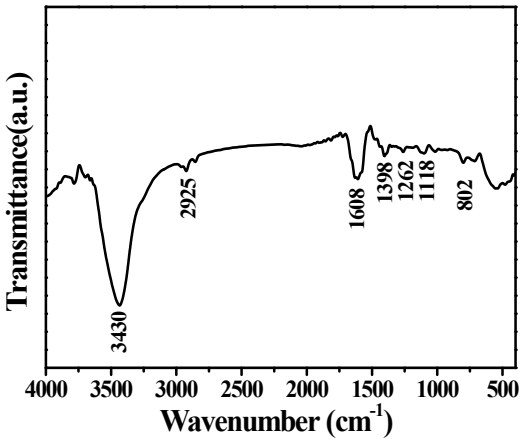

Fig. S2 FT-IR spectrum of NHC

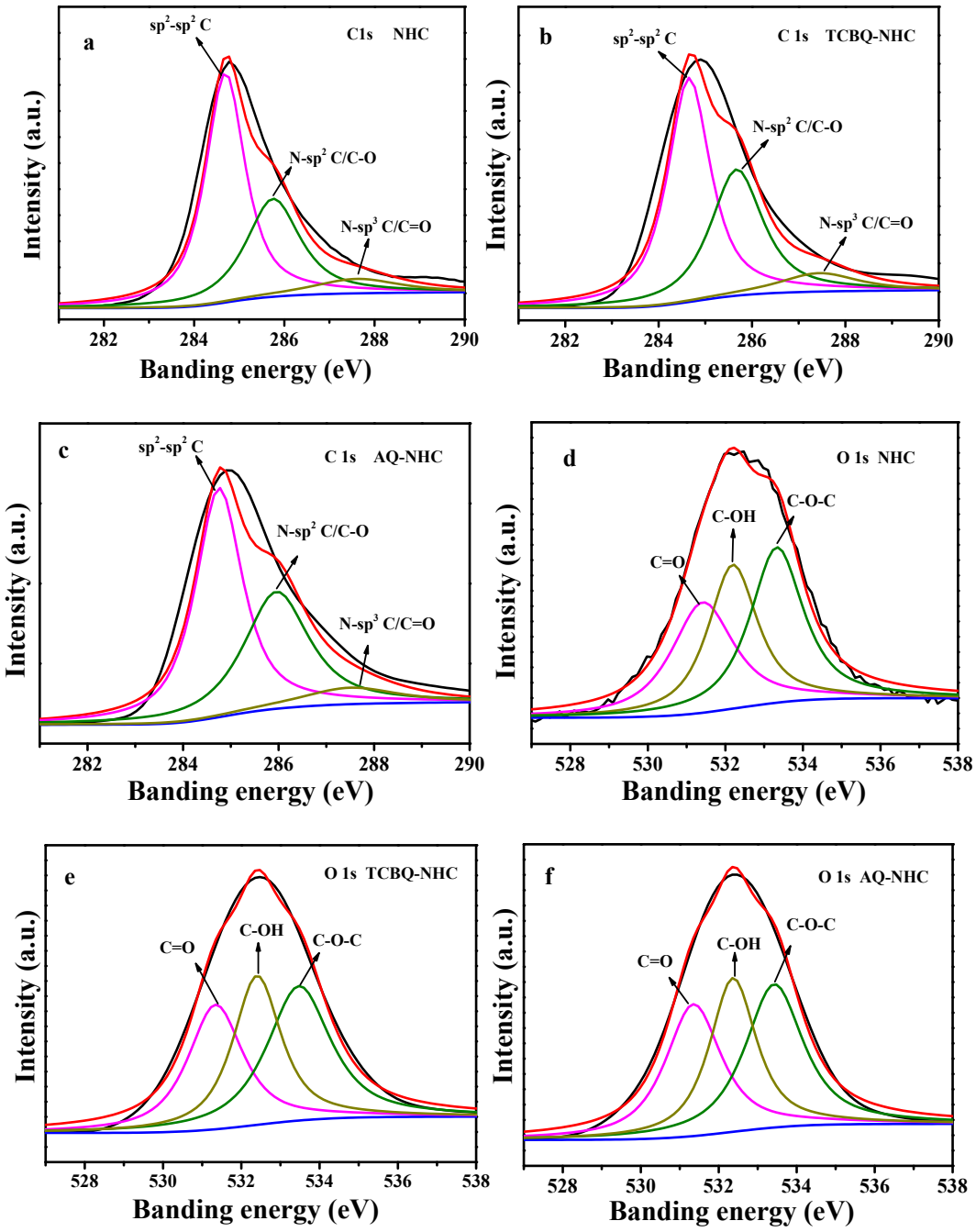

Fig. S3 C 1s regions of NHC, TCBQ-NHC and AQ-NHC (a-c), O 1s regions of NHC, TCBQ-NHC and AQ-NHC (d-f).

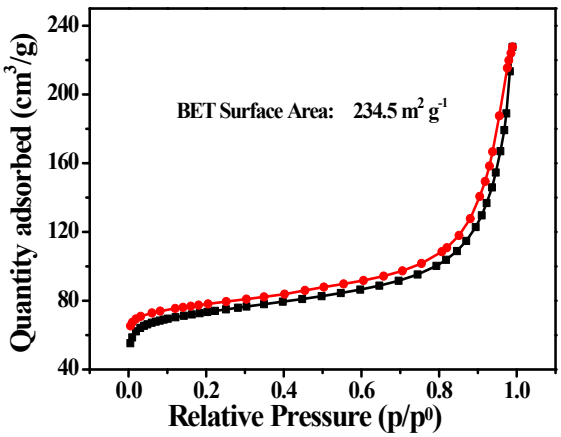

Fig. S4 Nitrogen adsorption/desorption isotherms of carbonized PANI/HCNTs.

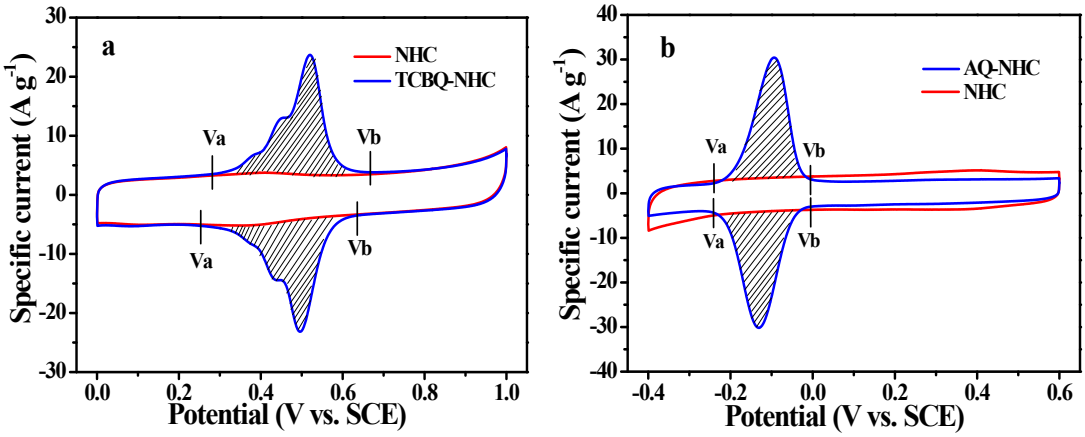

Fig. S5 CV curves of TCBQ-NHC (a) and AQ-NHC (b) at 20 mV s^{-1}.

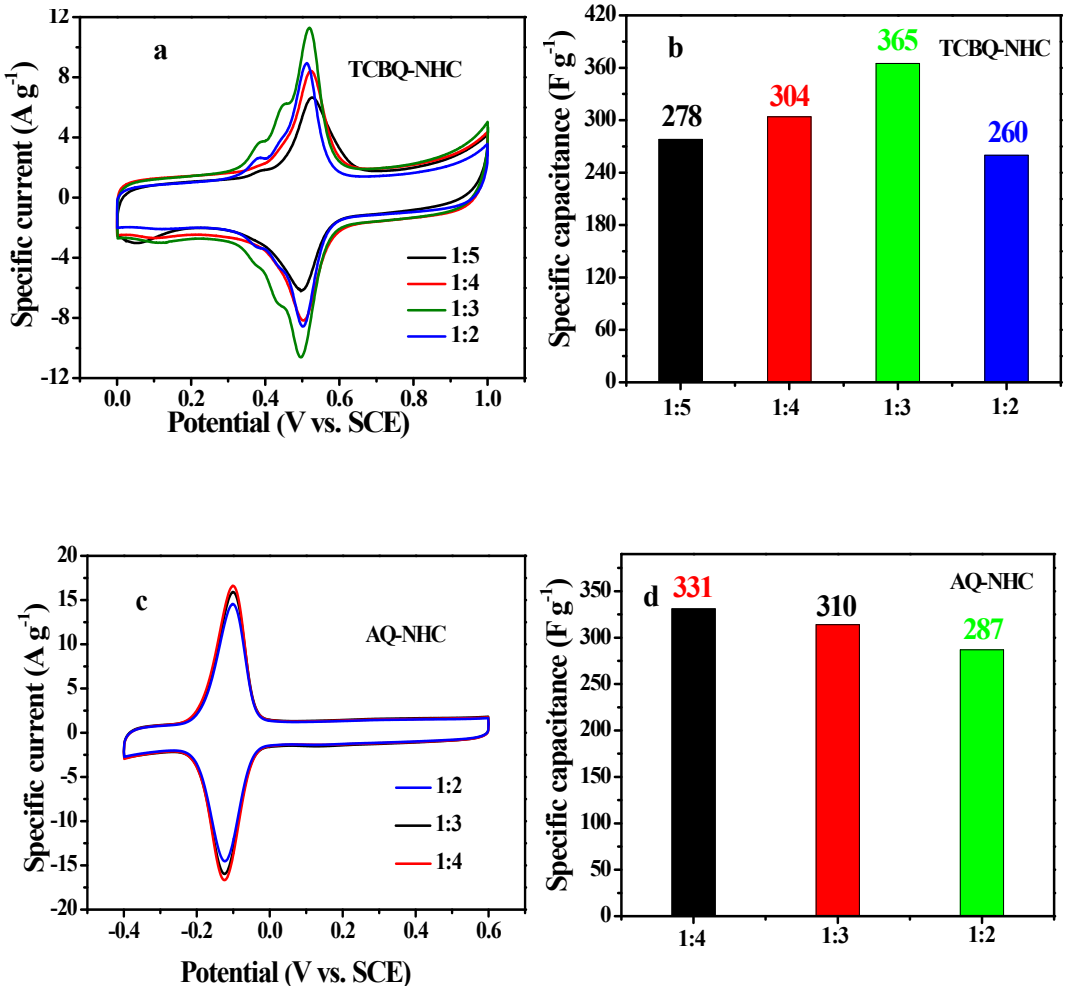

Fig. S6 the CV curves of TCBQ-NHC (a) and AQ-NHC (b) with different mass ratio at a scan rate of 10 mV s^{-1}, the specific capacitance of TCBQ-NHC (c) and AQ-NHC (d) with different mass ratio at the current of 1 A g^{-1}.

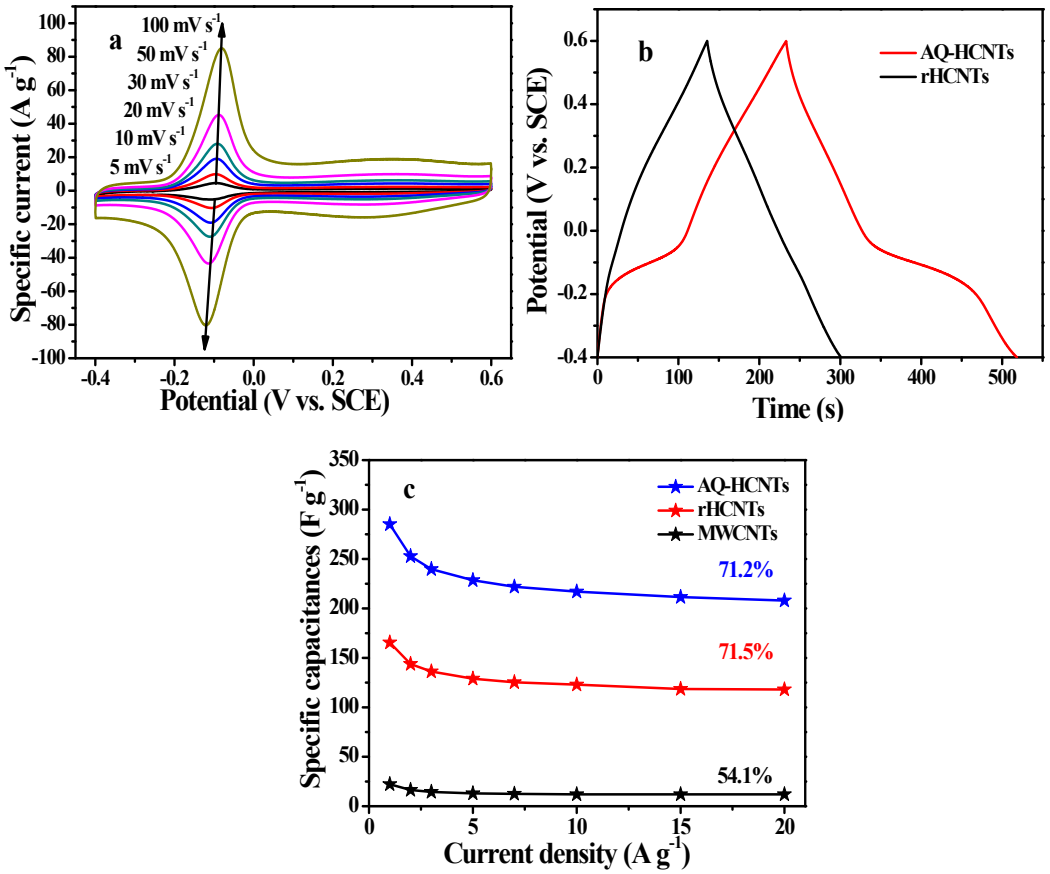

Fig. S7 the CV curves of AQ-HCNTs (a) at different scan rates, GCD curves of AQ-HCNTs (b) at current density of 1 A g^{-1} and specific capacitances of AQ-HCNTs (c) at various current density.

References

1 H. Wang, Y. Wang, Z. Hu, X. Wang, *ACS applied materials & interfaces*, 2012, **4**, 6827-6834.

2 L. Lin, M. Yeh, J. Tsai, Y. Huang, C. Sun and K. Ho, *Journal of Materials Chemistry A*, 2013, **1**, 11237.

3 G. Wang, Y. Ling, F. Qian, X. Yang, X. Liu and Y. Li, *Journal of Power Sources*, 2011, **196**, 5209-5214.

4 M. Rafiee, W.Lu, A. Thomas, A. Zandiatashbar, J. Rafiee, J. Tour and N. Koratkar, *Acs Nano*, 2010, **4**, 7415-7420.

5 B. Xiao, X. Li, X. Li, B. Wang, C. Langford, R. Li and X. Sun, *The Journal of Physical Chemistry C*, 2014, **118**, 881-890.

6 J. Zhang, Y. Wang, J. Zang, G. Xin, H. Ji, Y. Yuan, *Materials Chemistry and Physics*, 2014, **143**, 595-599.

7 J. Hernández, P. Laporta, F. Gutiérrez, M. Rubianesb, G. Rivasb, M. Martínez, *Electrochemistry Communications*, 2014, **39**, 26-29.

8 Q. Zhao, X. Wang, H. Xia, J. Liu, H. Wang, J. Gao, Y. Zhang, *Electrochimica Acta*, 2015, **173**, 566-574

9 T. Lin, I. Chen, F. Liu, C. Yang, H. Bi, F.Xu, F. Huang, *Science*, 2015, **350**, 1508-1513.

10 C. Zhong, S. Gong, Li. Jin, P. Li, Q. Cao, *Materials Letters*, 2015, **156**, 1-6.

11 M. Yeh, L. Lin, C. Sun, Y. Leu, J. Tsai, C. Yeh, R. Vittal and K. Ho, *The Journal of Physical Chemistry C*, 2014, **118**, 16626-16634

12 J. Zhao, H. Lai, Z. Lyu, Y. Jiang, K. Xie, X. Wang, Q. Wu, L. Yang, Z. Jin, Y. Ma, J. Liu and Z. Hu, *Advanced materials*, 2015, **27**, 3541-3545.

13 Y. Zhao, M. Liu, X. Deng, L. Miao, P. Tripathi, X. Ma, D. Zhu, , Z. Xu, Z. Hao, L. Gan, *Electrochimica Acta*, 2015, **153**, 448-45.

14 F. Zheng, Y. Yang and Q. Chen, *Nature communications*, 2014, **5**, 5261.

15 H. Wang, H. Yi, X. Chen, X. Wang, *Journal of Materials Chemistry A*, 2014, **2**, 1165-1173.

16 C. Wu, X. Wang, B. Ju, L. Jiang, H. Wu, Q. Zhao, *Journal of Power Sources*, 2013, **227**, 1-7.